International Journal of ChemTech Research
CODEN (USA): IJCRGG, ISSN: 0974-4290, ISSN(Online):2455-9555
Vol.9, No.06 pp 440-452, 2016

Detoxification of Methyl Orange and Trypan Blue Dyes by using Erbium loaded CuO nanoparticles

R. Sasikala, S. Kutti Rani*, K. Karthikeyan, D. Easwaramoorthy and I. Mohammed Bilal

Department of Chemistry, B. S. Abdur Rahman University, Vandalur, Chennai-600 048, India.

Abstract : Erbium loaded CuO nanoparticles (ECO NPs) were synthesized by a simple precipitation - thermal decomposition method and the catalyst was characterized by X-ray diffraction (XRD), field emission scanning electron microscopy (FE-SEM), energy dispersive spectrum (EDS), diffuse reflectance spectra (DRS), photoluminescence (PL), X-ray photoelectron spectroscopy (XPS) and BET surface area measurements. The XRD patterns proved that the ECO NPs exhibited monoclinic feature type as that of pure CuO. The ECO absorbed much more light in the UV region and lesser percentage of reflectance was noticed from PL spectra than CuO. The photo catalytic activity of CuO has been tested by the degradation of Methyl Orange (MO) and Trypan Blue (TB) under UV light irradiation was considerably enhanced their activity with Er loading. The Chemical Oxygen Demand (COD) measurement was used to confirm the mineralization of MO and TB. This catalyst was reusable and stable under UV light illuminations.
Key words : Er loaded CuO, Photocatalysis, UV light, Methyl Orange, Trypan Blue and Reusability

1. Introduction

CuO is a p-type semiconductor with a narrow band gap and has plentiful characteristics in nature, namely inexpensive, non-toxic, readily stored, low cost and easily produced. CuO has outstanding mesmerizing performance and hence it is expansively used for numerous applications such as heterogeneous photocatalysis, optical coating, solar cells, gas sensors and biosensors[1-4]. In addition to the catalytic reaction, the hasty recombination of electrons from the vacant conduction band with the positive holes of the valance band happened, which confines the effective degradation as well as decolourization of modern pollutants. A number of CuO (nanoparticles) NPs were used as a catalyst for the degradation of dyes with reasonable photocatalytic efficiencies[5, 6]. Although, for improving the photocatalytic activity of CuO, doping or loading with transition metal or rare earth metal and inner transition metals into CuO is a well-organized technique for diminishing the recombination rate of the photogenerated electron-hole pairs in the semiconductor oxide, the incorporation of RE^{3+} metal ions in CuO has the specialism of co-existence of semiconducting, optical and electrochemical properties[7, 8]. Unlike Lanthanides, Erbium is the metal that cover all the application such as dielectric constant, excellent chemical resistivity and also have high electron captures, higher activity in heterogenous catalytic activity in both organic transformation and environmental remediation's[9-11]. The adaptability, simplicity and easy operation conditions without chemical additives build the degradation as a promising method to eradicate textile dyes. There are many reports to be had formerly for doping of La^{3+}, Ce^{3+}, Gd^{3+} and Er^{3+} loaded metal oxides to improve their structural, electrical, optical and magnetic properties[12-16].

Superior catalytic activity of metal oxides using Er loaded CuO is not found in the literature. For that reason, we have selected two modern dyes such as Trypan Blue (TB) and Methyl Orange (MO). TB is an o-toludine based diazo dye, well known for its capability to selectively color the dead cells blue. MO which is commonly used in laboratory as indicator, especially MO used as an indicator in determination alkalinity of water. These dyes are used in extensive applications in textiles, paper, leather industries and research laboratories[17]. The most of the waste water from these industries is then overloaded with these type dyes. The presence of TB can cause considerable damage to the retina[18], carcinogenic and teratogenic effects in animals and probably humans[19, 20]. Where as MO also causes mutagenic and carcinogenic effects[21]. The photocatalytic degradation of TB and MO are available in the earlier reports[22-24], but there is no significant amount of work is carried out on the degradation process. Our present work is mainly focused on the preparation, characterization of Erbium loaded CuO NPs, and also about the photo catalytic activity of Tryphan Blue (TB) and Methyl Orange (MO) under UV light irradiation. The detoxifications of both dye molecules was also confirmed by chemical oxygen demand (COD) measurement.

2. Experimental

2.1. Materials

The commercial azo dyes, Trypan Blue, Methyl Orange (MB) from SD Fine, Oxalic acid dihydrate (99%) and copper nitrate pentahydrate (99%) were obtained from Himedia chemicals. Erbium (III) chloride hexahydrate (99.9%) were obtained from Spectrochem, commercial CuO (Himedia), $K_2Cr_2O_7$ (SD fine), Ag_2SO_4 (SD fine), $HgSO_4$ and $FeSO_4.7H_2O$ (Qualigens) were used as received. The double distilled water was used to prepare experimental solutions. The pH of the solutions before irradiation was adjusted using H_2SO_4 or NaOH.

2.2. Preparation of Er loaded CuO NPs

Er-loaded CuO was synthesized by simple precipitation-decomposition method. Aqueous solutions of Copper nitrate pentahydrate and oxalic acid were brought to their boiling points separately. The oxalic acid solution was mixed to the solution of copper nitrate; copper oxalate was formed. Then, 5 mL of 0.081 g $ErCl_3.6H_2O$ was added with the solution of copper oxalate suspension and this mixture was stirred for 1h at 70 °C. Then the mixture was cooled to room temperature, the Er containing copper oxalate (1 wt % Er related to CuO) was washed several times with distilled water, air-dried overnight and dried at 100°C for 5 hr. Calcinations of the mixed pricipitate at 450 °C for 5 hr resulted in the formation of ECO NPs. The Er loaded CuO NPs was collected and used for further analysis. This catalyst contained 1 wt% of Er. Using the same procedure 0.5, 1.5, and 2.0 wt% of Er loaded CuO were prepared. The bare CuO was prepared without addition of $ErCl_3$ by the same procedure with respective precursors.

2.3. Analytical methods

Powder X-ray diffraction patterns were obtained using an X'Per PRO diffractometer equipped with a CuKα radiation (wavelength 1.5406 Å) at 2.2 kW Max. Peak positions were compared with the standard files to identity the crystalline phase. The morphology of catalyst was examined using a JEOL JSM-6701F cold field emission scanning electron microscope (FE-SEM) equipped with OXFORD energy dispersive X-ray spectrum (EDS). Before FE-SEM measurements, the samples were mounted on a gold platform placed in the scanning electron microscope for subsequent analysis at various magnifications. Diffuse reflectance spectra were recorded using Shimadzu UV-2450. Photoluminescence (PL) spectra at room temperature were recorded using a Perkin Elmer LS 55 fluorescence spectrometer. The nanoparticles were dispersed in carbon tetrachloride and excited using light of wavelength 300 nm. The specific surface areas of the samples were determined through nitrogen adsorption at 77 K on the basis of BET equation using a Micromeritics ASAP 2020 V3.00 H. UV spectral measurements were done using Hitachi-U-2001 spectrometer. Chemical oxygen demand (COD) measurements were carried out by a reported procedure[25].

2.4. Photocatalytic experiments

For the degradation by UV-A light (365 nm), a Heber Multilamp-photoreactor HML MP 88 was employed [26]. This form consists of 8W medium pressure Hg vapour lamps set in similar and emitting 365 nm wavelength. It

has a reaction chamber with specially purposeful reflector made of polished aluminum and construct in cooling fan. It is offered a magnetic stirrer and 50 mL capacity reaction glass tubes. The light coverage length is 330 mm. The irradiation was carried out by means of four parallel 8W medium pressure Hg lamps. The solution with photo catalyst as well as dye solution was persistently aerated by a pump to supply oxygen and for absolute mixing of reaction solution and catalyst.

25 ml of dye solution (TB / MO) with the suitable concentration as well as the amount of catalyst was stirred for 30 min in the absence of light to prior to illumination in order to achieve maximum adsorption of dye on to the surface of the catalyst. It was observed that during the illumination time, there was no volatility of the solvent. At specific time intervals, 2-3 mL of sample was withdrawn and catalyst was detached by centrifugation. The changes in the concentration of dyes were observed from their characteristic absorption at UV and visible region using UV-Visible spectrophotometer. The absorbance at 200-400 nm correspond to the aromatic part of the dyes and the absence of absorbance indicates the degradation of dye molecule.

2.5. Chemical oxygen demand (COD) measurements

To verify the complete mineralization process, COD was determined using the following procedure. Sample was refluxed with $HgSO_4$, known volume of standard $K_2Cr_2O_7$, Ag_2SO_4 and H_2SO_4 for two hours and titrated with standard ferrous ammonium sulfate (FAS) using ferroin as indicator. A blank titration was carried out with distilled water instead of dye sample. COD was determined using the following equation.

$$\text{COD} = \frac{(\text{Blank titre value - dye sample titre value}) \times \text{normality of FAS} \times 8 \times 1000}{\text{Volume of sample}} \quad \ldots\ldots (1)$$

3. Results and Discussion

3.1. Characterization of catalyst

Primary analysis of photocatalytic degradations of TB and MO with different wt% Er on CuO catalysts was carried out. As reported earlier, this heterogeneous photocatalysis follows *pseudo*-first order kinetics[27]. *Pseudo*-first order rate constants determined for 0.5, 1.0, 1.5 and 2.0 wt% Er loaded CuO were 0.071, 0.091, 0.079 and 0.060 min^{-1} for TB, 0.052, 0.075, 0.0580 and 0.053 min^{-1} for MO. From this results 1 wt% of Er loaded CuO catalyst was found be most efficient for both TB and MO dyes. Hence, this catalyst was characterized by XRD, FE-SEM, EDS, DRS, PL, XPS and BET surface area measurements.

XRD patterns of pure and Er-loaded CuO (1 wt%) nanoparticles are given in Fig. 1. The reflections at 2θ of 35.45°, 38.73°, 42.50°, 48.92°, 61.99° and 66.49° are attributed to monoclinic phase of CuO[28] (JCPDS Card 048-1548) (Fig.1a). The characteristic reflections relating to the Erbium in the XRD pattern of Er-loded CuO NPs is absent (Fig.1b). This can be due to the very small amount of catalyst and an appropriate incorporation of erbium ions in the CuO lattice[29]. The inset of Fig. 1 shows that the peak corresponding to ECO NPs was slightly shifted to a lower angle side, which revealed that the Er was loaded on the surface of CuO material[29].

The average crystallite size of pure and Er-loaded CuO samples calculated from the Scherrer's equation.

$$D = \frac{K\lambda}{\beta \cos \theta}$$

Where D is the crystal size of the catalyst, K is a dimensionless constant, λ is the wavelength of the X-rays, β is the full width at half-maximum (FWHM) of the diffraction peak and θ is the diffraction angle. Since this equation, the crystallite size of bare CuO and Er-loaded CuO was calculated using the sharpest reflection are 25 nm and 16 nm, respectively.

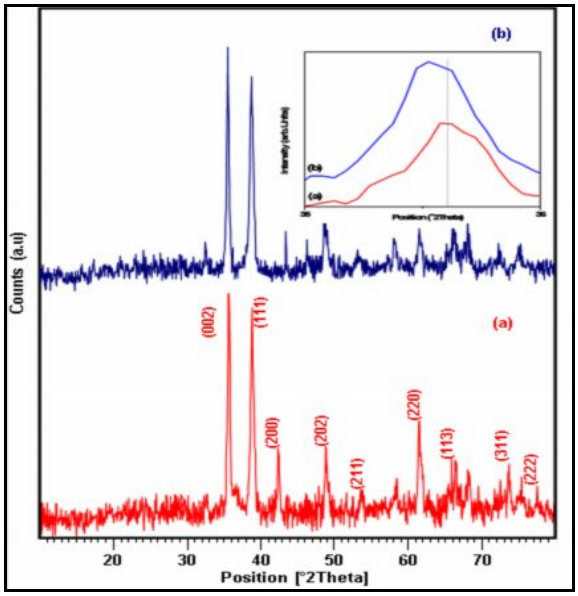

Fig. 2. XRD patterns of a) bare CuO and b) ECO NPs (The inset figure shows Magnification of XRD patterns of (a) bare CuO and (b) ECO NPs)

Structure and morphology of the catalyst were the most imperative factors that manipulate the catalytic activity. Fig. 2 shows the FE-SEM images of both CuO (Fig. 2a & 2b) and ECO (Fig. 2c & 2d) at different magnifications with different locations. The ECO in Figs. 2c & 2d exhibits particles with spherical as well as flake like structures, uniform distribution and slight agglomeration also appeared in ECO. The composition of ECO was analyzed with EDS and shown in Fig. 3. The results from EDS spectra states that the ECO contains Cu, Er and O.

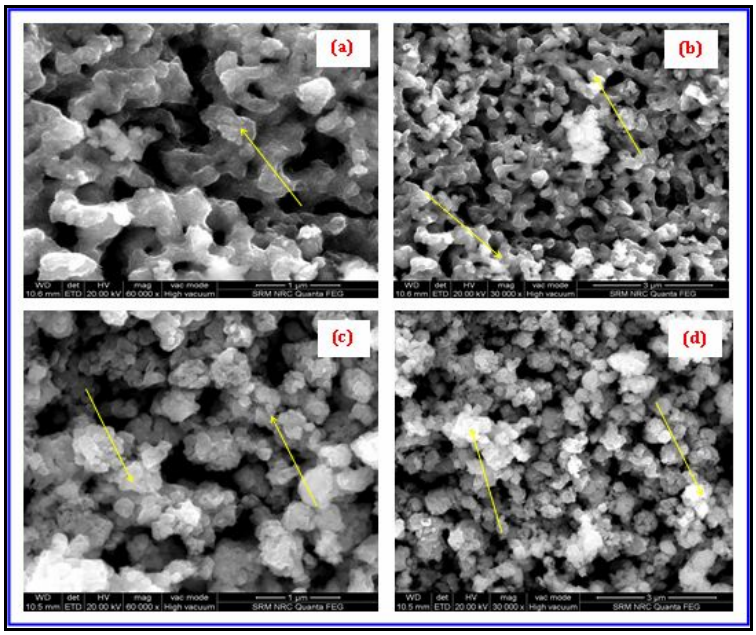

Fig. 2. FE-SEM images of bare CuO and ECO NPs a) bare CuO (1 µm), b) bare CuO (3 µm)c) ECO (1 µm) d) ECO (3 µm).

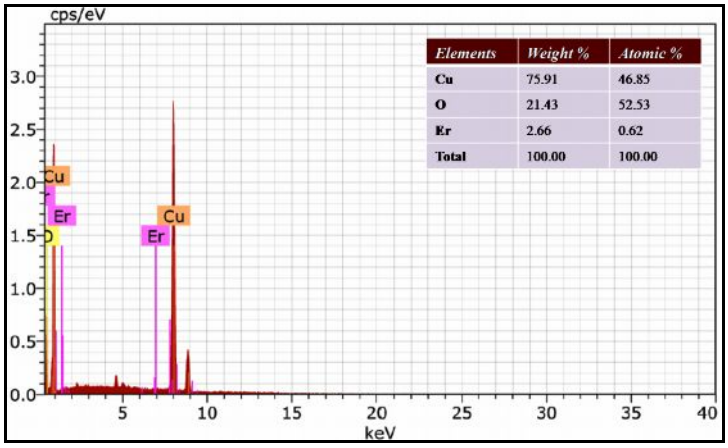

Fig. 3. EDS of ECO NPs

The UV–vis diffuse reflectance spectra of bare CuO and ECO samples are shown in Fig. 4. It is conspicuous that the diffuse reflectance spectra of ECO exhibit a higher absorption in the region of 200-800 nm when compared to bare CuO. Photoluminescence (PL) spectra are repeatedly used to monitor the efficiency of charge carrier trapping, reposition, as well as to be aware of the fate of photogenerated e^-/h^+ pairs in semiconductor oxide. The emission spectra of bare CuO and ECO (Fig. 5a & 5b) shows evidence of faintly typical green emission in the range of 330–480 nm. It is acknowledged that the luminescence spectrum of a semiconductor could be proficient to the radiative recombination process of generated e^- - h^+ pairs. In view of that, the PL intensity of ECO is reduced which might signify a low recombination rate of the e^-/h^+ pairs and high photon efficiency of the catalyst. These factors are attributed for the enhancement of catalytic activity in ECO NPs.

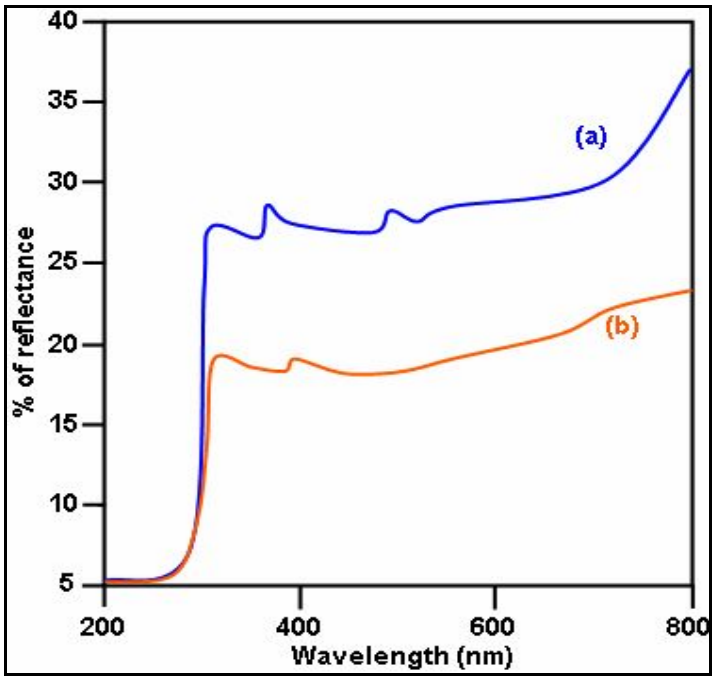

Fig. 4. DRS of a) bare CuO and b) ECO NPs

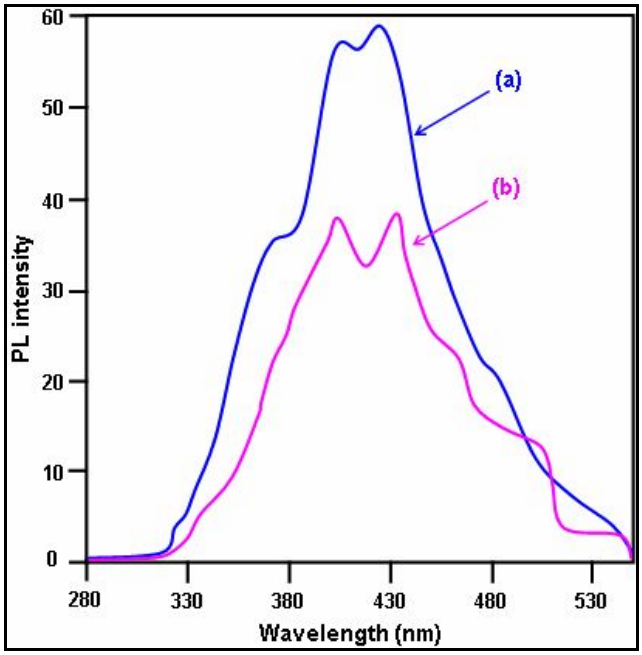

Fig. 5. Photoluminescence spectra of a) bare CuO and b) ECO NPs

The presence of Er 4d in the ECO NPs is established using XPS spectra. Fig. 6 demonstrate the XPS survey spectra of the 1 wt% erbium loaded CuO NPs. Fig. 6(a) shows the whole spectrum, where the elements Cu, O, C and Er are labelled to subsequent binding energies. In the XPS spectra the binding energies are calibrated by taking C 1s peak as reference.

Fig. 6(b)–(d) shows the magnified spectra of Cu 2p, O 1s and Er 4d peaks respectively. In Fig. 6(b), the binding energies of 934.7 eV and 954.7 eV are on behalf of Cu $2p_{3/2}$ and Cu $2p_{1/2}$ respectively. These values match well with the data reported for the Cu 2p in CuO[30]. Additionally, the shake-up satellite peaks situated at 944.2 eV and 963.0 eV are characteristic of materials having a d^9 configuration[31]. The strong shake-up satellites recorded in the ECO NPs confirm the Cu^{2+} oxidation state and rule out the probability of the survival of a Cu_2O phase[30]. In Fig. 6(c), the peak corresponding to O 1s level is fitted in to two peaks at 530.2 eV and 532.0 eV. The first one with lower energy (530.2 eV) designate the presence of intrinsic oxygen in CuO and the other at 532.0 eV is accredited to chemisorbed oxygen of the surface hydroxyl, carbonates, adsorbed water or chiefly due to surface contamination[32]. The peak at 169.8 eV in Fig. 6(a) and (d) indicates the presence of Er in the catalyst. The binding energy 169.8 eV corresponds to the Er 4d level and thus the trivalent oxidation state of erbium in the sample is confirmed[29].

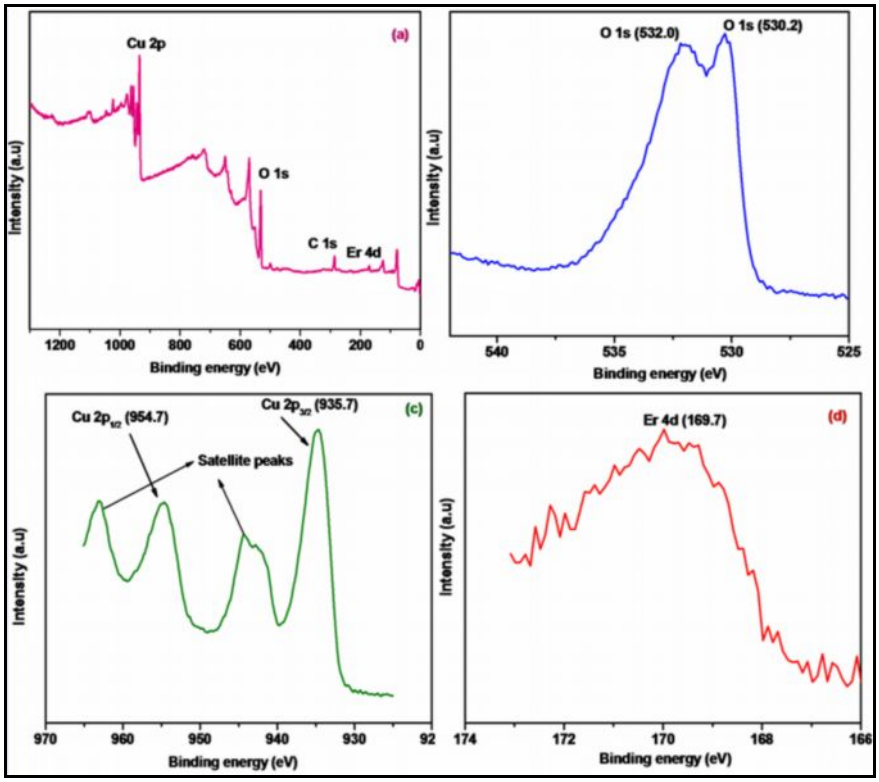

Fig. 6. XPS spectrum of ECO NPs: (a) Survey spectrum, (b) O 1s peak, (c) Cu 2p peak, and (d) Er 4d peak.

Generally, the surface area of the catalyst is the most important factor influencing the catalytic activity. The BET surface area of CuO and ECO was determined using the nitrogen gas adsorption method. Beginning of the adsorption–desorption data analyses, the textural properties of the synthesized photocatalyst CuO and ECO were obtained (Table 1). The BET surface area of ECO (6.86 m^2g^{-1}) was higher when compared to CuO (1.82 ($m^2 g^{-1}$). From these results, it clearly indicates higher surface area of the catalyst enhances its catalytic activity.

Table 1. Surface properties of the catalysts.

Properties	bare CuO NPs	ECO NPs
BET surface area	1.82 ($m^2 g^{-1}$)	6.86 ($m^2 g^{-1}$)
Total pore volume (single point)	0.01 ($cm^3 g^{-1}$)	0.04 ($cm^3 g^{-1}$)

3.2. Photo detoxification TB and stability of the catalyst

For the photocatalysis reaction to occur, both catalyst and a light source are more essential. A control experiment was carried out on the irradiation of TB under only UV light, in the presence of ECO with and without light irradiation, as shown in Fig. 7. Here there was no degradation observed in the subsistence of UV light (curve d). Since the above results shows that there was insignificant degradation (0.2 %) when the reaction was permissible to occur in the presence of UV light without any ECO catalyst. Besides to that about less than 1% decrease in dye concentration occurred due to adsorption for the same experiment execute with ECO in the absence of UV light (curve e). Almost complete degradation was accomplished (100 %) in presence ECO with UV light (5 hr) (curve a). While the photocatalysts bare CuO, and commercial CuO were used under similar conditions only 82.9 (curve b) and 77.9 (curve c) percentages of degradation occurred, respectively. From above the results clearly shows that ECO is more proficient in TB dye degradation than other prepared and commercial catalysts.

Usually, semiconductor photocatalyst life span is an important constraint of the catalytic process because of its use for a longer period of time show the way to a huge cost reduction of the treatment. For this incentive, catalyst life time was tested again and again by carrying out the degradation with the used catalyst. The results for three

cycles of the catalyst are shown in Fig. 8. Degradation efficiencies at first, second, and third cycles are 100, 99.6 and 97.3% respectively. ECO exhibited outstanding photostability without any noticeable loss of photocatalytic activity even at third cycles. These results indicate that ECO catalyst remains effective and reusable under UV light.

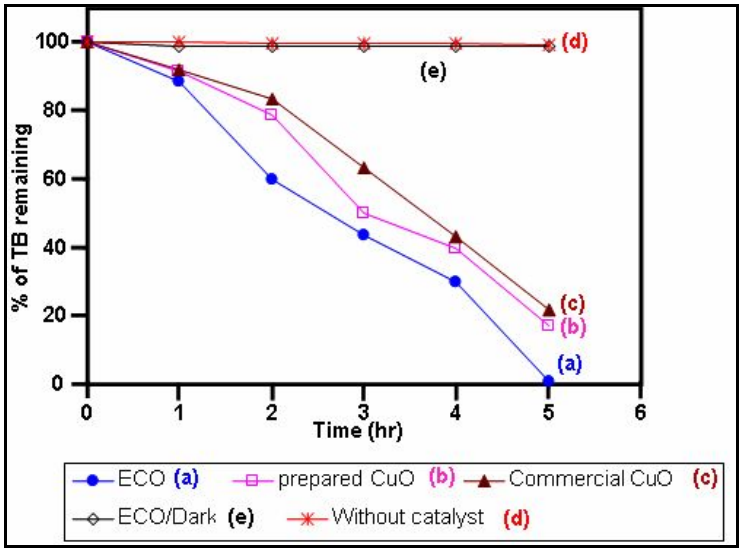

Fig. 7. Photodegradability of TB; [TB] = 2×10^{-4} M, catalyst suspended = 1 g L^{-1}, pH = 7, airflow rate = 8.1 mL s^{-1}, $I_{UV} = 1.381 \times 10^{-6}$ einstein L^{-1} s^{-1}

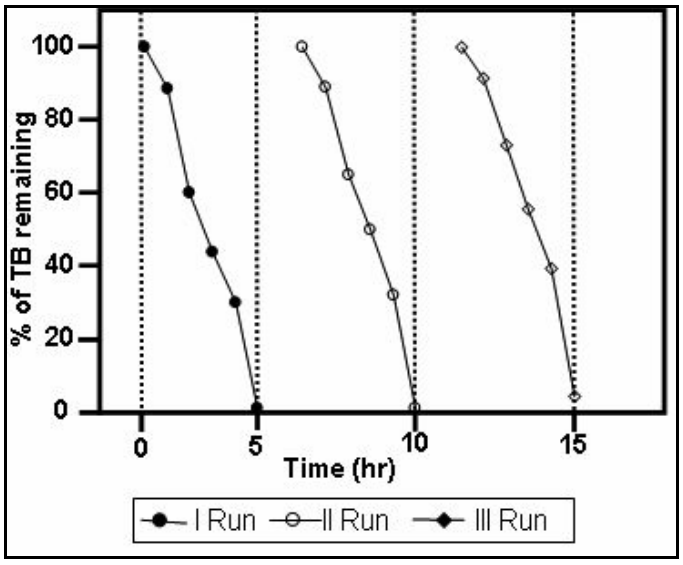

Fig. 8. Catalyst reusability, [TB] = 2×10^{-4} M, 1 wt% ECO suspended = 1 g L^{-1}, pH = 7, airflow rate = 8.1 mL s^{-1}, $I_{UV} = 1.381 \times 10^{-6}$ einstein L^{-1} s^{-1}

3.3. Photo detoxification of MO and stability of the catalyst

After getting equilibrium in dark, according to the desorption test from the adsorbed sample, approximately 1 % of MO (curve b) was adsorbed this may be due to adsorption of the dye on the surface of the catalyst (Fig. 9). There was insignificant degradation (0.2 %) when the reaction was allowed to take place in the presence of UV light without any catalyst (curve c). It was found that the appearance of the catalyst before and after use was the same (not shown here). It reveals that adsorbed MO has been degraded completely (curve a). From these interpretations clearly reveal that UV light and photocatalyst are crucial for effective devastation of MO dye. When the photocatalyst of bare CuO and commercial CuO were used under same conditions only 80.9 (curve d) and 80.6 (curve e) percentages of degradations occurred, respectively. This shows that UV/ ECO process is more efficient in MO dye degradation than other processes.

In order to determine the firmness of photocatalyst during the photo catalytic detoxification of MO, ECO catalyst was used repeatedly for three runs. The results are shown in Fig. 10. There was no considerable loss of photocatalytic activity up to third run (91.3%). The recovered photocatalyst gives us an idea about the same color as the newly prepared catalyst. This indicates the stability of the photocatalyst during the photocatalytic reaction.

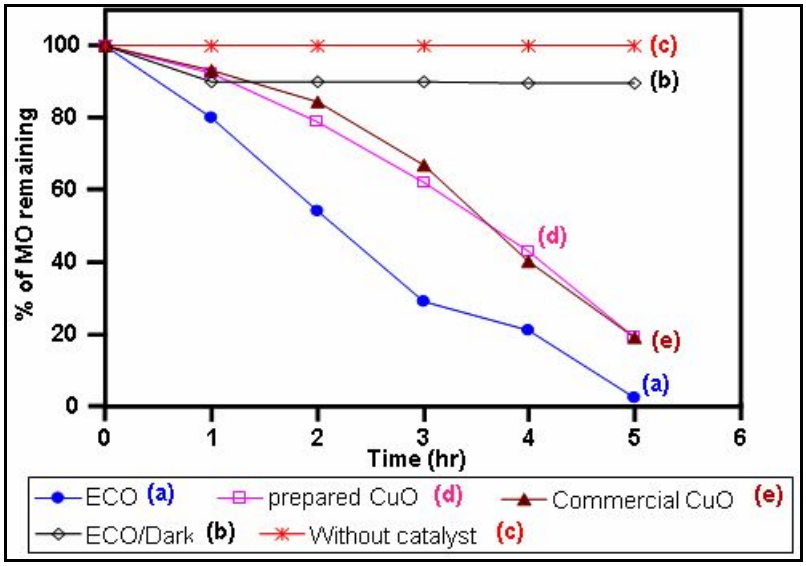

Fig. 9. Photodegradability of MO; [MO] = 5×10^{-4} M, catalyst suspended = 1 g L^{-1}, pH = 7, airflow rate = 8.1 mL s^{-1}, $I_{UV} = 1.381 \times 10^{-6}$ einstein L^{-1} s^{-1}

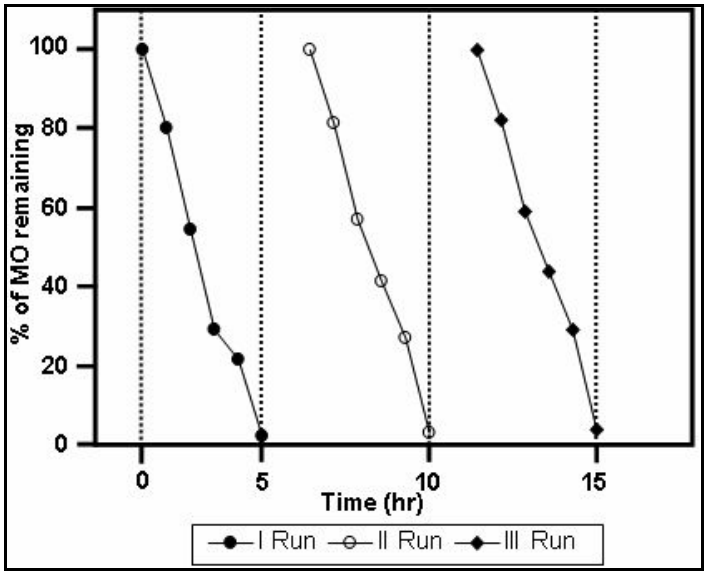

Fig. 10. Catalyst reusability, [MO] = 5×10^{-4} M, 1 wt% ECO suspended = 1 g L^{-1}, pH = 7, airflow rate = 8.1 mL s^{-1}, $I_{UV} = 1.381 \times 10^{-6}$ einstein L^{-1} s^{-1}

3.4. UV-visible spectra of the dyes at different time of irradiation

Fig. 11 and 12 showed the perceptible changes in the absorbance spectra of two azo (TB & MO) dyes with ECO photocatalyst at different time intervals under UV light illumination. The absorbance at the utmost absorption peak (above 400 nm) is due to n→π* transition of the -N=N- and hydrazone forms, which is reason for the colour of azo dyes. The absorbance at 200–400 nm was allowed to π→π* transition of benzene rings, it is representing the aromatic part of azo dyes, and its disappearance due to the degradation of aromatic part of the dye[33]. After the reaction time was prolonged, all the peaks in dye molecules decreased progressively. New peaks are not showed during irradiation in the analyzed wavelength range. It designated that the main chromophores and aromatic part in the original dye solution were overwhelmed in the presence of ECO under

UV light illumination. In addition, these spectra also reveal that intermediates do not absorb the analytical wavelengths.

3.5. COD analysis TB & MO dyes

Chemical Oxygen Demand (COD) is an important factor for evaluating the concentration of untreated contaminants in water resources. Because the degradation of organic compounds requires oxygen, their concentrations can be unsurprising by the amount of oxygen required for the degradation of water resources[34]. The mineralization of these dyes (TB and MO) was reported by measuring the COD values by different time interval of illuminated solution under appropriate UV light conditions. The percentages of COD reduction at different times of irradiation are presented in Table 2. About 100 % (TB) and 93.4 % (MO) of COD reduction were observed for these dyes at respective time of irradiation. It clearly indicates the complete mineralization of dye molecules.

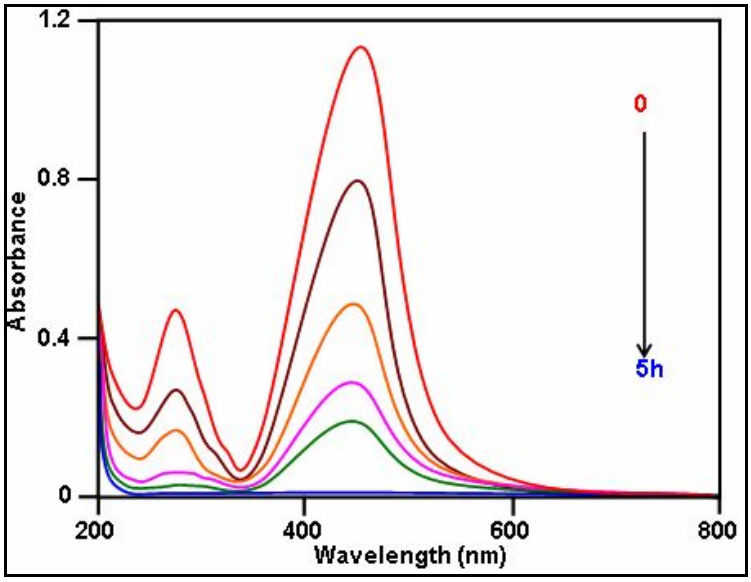

Fig. 11. The changes in UV-vis spectra of TB on irradiation with UV light in the presence ECO: [TB] = 2×10^{-4} M; pH = 7; catalyst suspended = 1 g L^{-1}; airflow rate = 8.1 mL s^{-1};

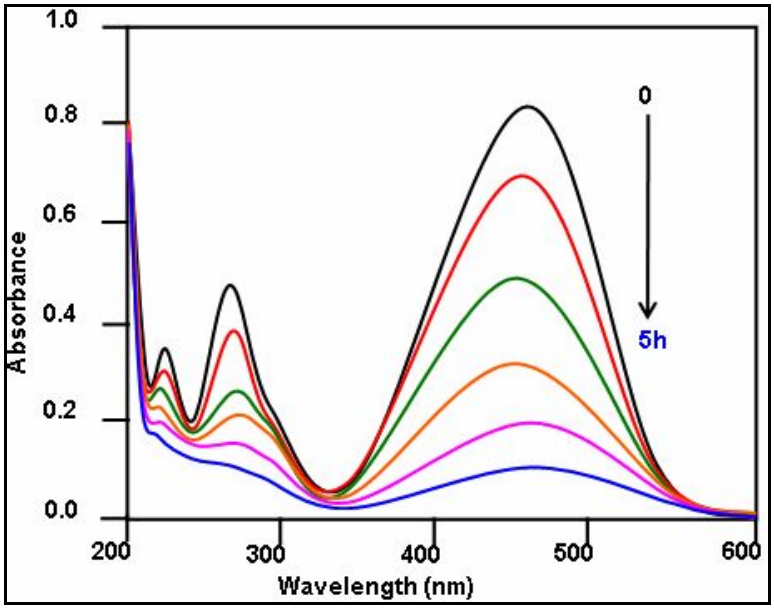

Fig. 12. The changes in UV-vis spectra of MO on irradiation with UV light in the presence ECO: [MO] = 5×10^{-4} M; pH = 7; catalyst suspended = 1 g L^{-1}; airflow rate = 8.1 mL s^{-1}

Table 2. COD measurements

Time (hr)	COD removal (TB)[a]	COD removal (MO)[b]
0	0	0
1	17.9	13.5
3	60.0	56.0
5	98.1	93.4

[a] [TB] = 2×10^{-4} M; 1 wt% ECO suspended = 1 g L^{-1}; pH = 7; airflow rate = 8.1 mL s^{-1}; I_{UV} = 1.381×10^{-6} einstein L^{-1} s^{-1}.

[b] [MO] = 5×10^{-4} M; 1 wt% ECO suspended = 1 g L^{-1}; pH = 7; airflow rate = 8.1 mL s^{-1}; I_{UV} = 1.381×10^{-6} einstein L^{-1} s^{-1}.

3.6. Mechanism of dye degradation

When semiconductor is illuminated by light radiation, a valence band electron (VB) goes to conductance band (CB) leaving a hole in valence band (Scheme. 1). On the whole these electron-holes are recombined to diminish the photocatalytic activity of the semiconductor. But the presence of 'Er' catches the electron from CB of CuO, which represses the e^- - h^+ recombination. It shows, the photocatalytic activity of ECO photocatalyst was greater to that of bare CuO and commercial CuO photocatalyst. In addition to that the O_2 adsorbed on the surface of photocatalyst can trap the photogenerated electron[35, 36]. Moreover, the trapping nature of Er sites molecules are subsequently transferred to the surrounding adsorbed O_2 to produce more number of superoxide radical anion ($O_2^{\bullet-}$) and at the same time VB holes of CuO react with water to produce highly reactive hydroxyl ($^{\bullet}OH$) radical. The highly reactive $O_2^{\bullet-}$ and $^{\bullet}OH$ are used for the degradation of both the dye molecules.

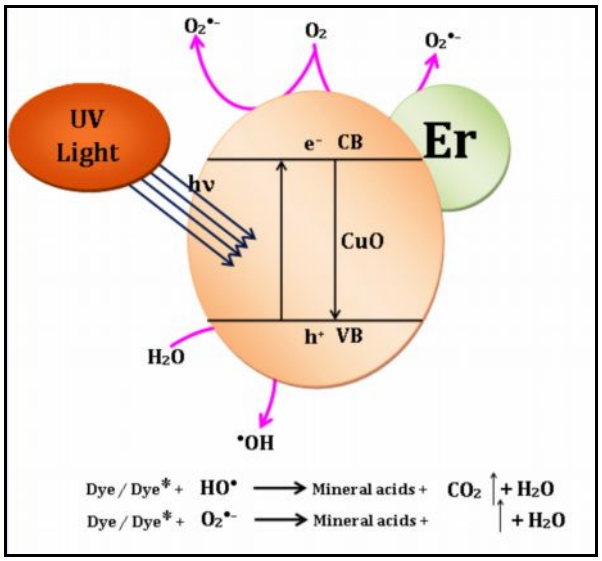

Scheme 1. Mechanism of degradation of dyes by ECO NPs

4. Conclusion

A new Er loaded CuO was synthesized by simple precipitation- decomposition method and characterized by XRD, FE-SEM, EDS, DRS, PL and BET surface area measurements. ECO has higher absorption than bare CuO in entire visible region. The PL spectra reveal the suppression of recombination of the photogenerated electron-hole pairs by the Er loading on CuO. ECO was found to be highly efficient than both bare and commercial CuO for degradation of dyes under UV light illumination. This catalyst was found to be more stable. COD measurements authenticate that the almost complete mineralization of all the dye molecules. A mechanism is proposed for the

superior photocatalytic activity of the ECO. This process using ECO photocatalytic material would be more useful for industrialized waste water treatment as well as some organic transformation due to the advantages of its effortlessness, economical and recyclability.

Acknowledgements

The authors are grateful to the DST-SERB (Project no. SB/FT/CS-033/2013) for financial support and author R. Sasikala. thanks B S Abdur Rahman University for providing a fellowship.

References

1. Bhaumik A, Shearin AM, Patel R, Ghosh K. Significant enhancement of optical absorption through nano-structuring of copper based oxide semiconductors: possible future materials for solar energy applications. Phys. Chem. Chem. Phys., 2014, 16: 11054-11066.
2. Ko J, Kim S, Hong J, Ryu J, Kang K, Park C. Synthesis of graphene-wrapped CuO hybrid materials by CO2 mineralization. Green Chem., 2012, 14: 2391–2393.
3. Wanga X, Hua C, Liu H, Du G, He X, Xi Y. Synthesis of CuO nanostructures and their application for nonenzymatic glucose sensing. Sensors Actuator B-Chemical., 2010, 144: 220-222.
4. Yang C, Su X, Wang J, Cao X, Wang S, Zhang L. Facile microwave-assisted hydrothermal synthesis of varied shaped CuO nanoparticles and their gas sensing properties. Sens. Actuators B: Chemical., 2013, 85: 159-165.
5. Kim SH, Umar A, Rajesh Kumar, Ibrahim AA, Kumar G. Facile synthesis and photocatalytic activity of cocoon-shaped CuO nanostructures., 2015, 156: 138-141.
6. Mageshwari K, Sathyamoorthy R, Park J. Photocatalytic activity of hierarchical CuO microspheres synthesized by facile reflux condensation method. Powder Technol., 2015, 278: 150-156.
7. Xiao Q, Si Z, Zhang J, Xiao C, Tan X. Photoinduced hydroxyl radical and photocatalytic activity of samarium-doped TiO_2 nanocrystalline. J. Hazard. Mater., 2008, 150: 62–67.
8. Subash B, Krishnakumar B, Swaminathan M, Shanthi M, Synthesis and characterization of cerium-silver co-doped zinc oxide as a novel sunlight-driven photocatalyst for effective degradation of Reactive Red 120 dye. Mater. Sci. Semicond. Process., 2013, 13: 1070–1078.
9. Hubbard KM, Espinoz BF. Corrosion-resistant erbium oxide coatings by organometallic chemical vapor deposition. Thin Solid Films., 2000, 366: 175-180.
10. D. Xue, K. Betzler, H. Hesse. Dielectric constants of binary rare-earth compounds. J. Phys. Condens. Matter., 2000, 12: 3113-3118.
11. G. Adachi, N. Imanaka, The binary rare earth oxides. Chem. Rev. 1998, 98, 1479-1514.
12. P. Dhatshanamurthi, B. Subash, M. Shanthi. Investigation of UV-A light photocatalytic degradation of an azo dye in the presence of CdO-TiO_2 coupled semiconductor. Mater. Sci. Semicond. Process. 2015, 35, 22–29.
13. P.V. Korake, A.N. Kadam, K.M. Garadkar. Photocatalytic activity of Eu^{3+} doped ZnO nanorods synthesized via microwave assisted technique. J. Rare Earths, 2014, 32, 306–313.
14. Shijina K, Megha U, Varghese G. Ultraviolet multi-peak emissions of mono-dispersed polymer capped ZnNiO nanocomposites. J. Lumin. 2014, 145, 219–223.
15. Eskandarloo H, Badiei A, Behnajady MA, Ziarani GM. Ultrasonic-assisted degradation of phenazopyridine with a combination of Sm-doped ZnO nanoparticles and inorganic oxidants, Ultrason Sonochem., 2016, 28: 169–177.
16. Stengl V, Bakardjieva S, Murafa N. Preparation and photocatalytic activity of rare earth doped TiO_2 nanoparticles. Mater. Chem. Physics., 2009, 114: 217–226.
17. Zollinger H, Synthesis, Properties of Organic Dyes and Pigments. In: Color Chemistry. New York, USA: VCH Publishers; 1987, 92-102.
18. Veckeneer M, van Overdam K, Monzer J, Kobuch K, van Marle W, Spekreijse H, van Meurs J. Ocular toxicity study of trypan blue injected into the vitreous cavity of rabbit eyes. Graefes Arch. Clin. Exp. Ophthalmol., 2001, 239: 698-704.
19. Turbow MM, Teratogenic effect of trypan blue on rat embryos cultivated in vitro. Nature, 1965, 206: 637.

20. Waddington CH, Perry MM, Teratogenic effects of trypan blue on amphibian embryos. J. Embryol. Exp. Morph., 1956, 4: 110-119.
21. Sylvia Devi H, David Singh T, Synthesis of Copper Oxide Nanoparticles by a Novel Method and its Application in the Degradation of Methyl Orange, Advance in Electronic and Electric Engineering., 2014, 4: 83-88.
22. Velmurugan R, Krishnakumar B, Swaminathan M. Sonochemical synthesis and characterization of barium fluoride–titanium dioxide nanocomposites and activity for photodegradation of Trypan Blue dye, Materials Science in Semiconductor Processing., 2014, 27: 654–664.
23. Nenavathu BP, Krishna Rao AVR, Goyal A, Kapoor A, Dutta R. Synthesis, characterization and enhanced photocatalytic degradation efficiency of Se doped ZnO nanoparticles using trypan blue as a model dye. Applied Catalysis A: General., 2013, 459: 106–113.
24. Ejhieh AN, Shamsabadi MK, Comparison of photocatalytic efficiency of supported CuO onto micro and nano particles of zeolite X in photodecolorization of Methylene blue and Methyl orange aqueous mixture. Applied Catalysis A: General., 2014, 477: 83–92.
25. B. Subash, B. Krishnakumar, M. Swaminathan, M. Shanthi. Highly efficient, solar active and reusable photocatalyst, Zr loaded Ag-ZnO for Reactive Red 120 dye degradation with synergistic effect and dye sensitized mechanism, Langmuir, 29 (2013) 939–949.
26. K. Muthu, K. Selvam, B. Krishnakumar, M. Swaminathan, Energy-efficient regeneration of ketones from oximes using semiconductor photocatalysts Appl. Catal. A.358 (2009) 259–263.
27. B. Subash, B. Krishnakumar, M. Swaminathan, M. Shanthi, β-Ag_2S–ZnO as a novel sunshine photocatalyst for the effective degradation of RR 120 dye, Powder Technol. 249 (2013) 49–59.
28. A.S. Ethiraj, D.J. Kang, Synthesis and characterization of CuO nanowires by a simple wet chemical method, Nanoscale Res. Lett. 7 (2012) 70-74.
29. N.K. Divya, P.P. Pradyumnan, Solid state synthesis of erbium doped ZnO with excellent photocatalytic activity and enhanced visible light emission, Materials Science in Semiconductor Processing 41 (2016) 428–435.
30. R. Sasikala, S. Kutti Rani, D. Easwaramoorthy, K. Karthikeyan, Lanthanum loaded CuO nanoparticles: synthesis and characterization of a recyclable catalyst for the synthesis of 1,4-disubstituted 1,2,3-triazoles and propargylamines, RSC Adv. 5 (2015) 56507–56517.
31. C.K. Wu, M. Yin, S. O'Brien and J. T. Koberstein, Quantitative Analysis of Copper Oxide Nanoparticle Composition and Structure by X-ray Photoelectron Spectroscopy, Chem. Mater. 18 (2006) 6054-6058.
32. Z. Zhao, J.Song, J. Zheng, J. Lian. Optical properties and photocatalytic activity of Nd-doped ZnO powders. Trans. Nonferr. Met. Soc. China. 2014, 24, 1434–1439.
33. B. Subash, B. Krishnakumar, M. Swaminathan, and M. Shanthi, ZnS−Ag−ZnO as an Excellent UV-Light-Active Photocatalyst for the Degradation of AV 7, AB 1, RR 120, and RY 84 Dyes: Synthesis, Characterization, and Catalytic Applications, Ind. Eng. Chem. Res. 2014, 53, 12953−12963.
34. L.D. Xi, Y.S. Song, X. Liu, Methods in Environmental Monitoring, Advanced Education Press: Beijing (1996) 70−80.
35. B. Subash, B. Krishanakumar, R. Velmurugan, Swaminathan M.; Shanthi, M. Synthesis of Ce co-doped Ag-ZnO Photocatalyst with excellent performance for NBB dye degradation under natural sunlight illumination, Catal. Sci. Technol. 2 (2012) 2319–2326.
36. G.M. Mura, M.L. Ganadu, P. Lombardi, G. Lubinu, M. Branca, V. Maida, A preliminary comparison between hydrogenase and oxygen as electron acceptors in irradiated aqueous dispersion of titanium dioxide J. Photochem. Photobiol. A. 148 (2002) 199–204.

*****